A Combined MBPC/ 2 DOF H_∞ Controller for a Quad Rotor UAV

Ming Chen [*] Mihai Huzmezan [†]

Department of Electrical and Computer Engineering
University of British Columbia
Vancouver, BC, Canada, V6T 1Z4

Abstract

Unmanned Aerial Vehicles (UAVs) have generated considerable interest in the control and commercial community for several decades due to their advantages over manned systems. In this work we focus on the nonlinear modelling of a quad rotor UAV. An experimental system including a flying mill, a DSP system, a programmed microprocessor and a wireless transmitter have been used to test the flight controller. Based on the nonlinear model, an H_∞ loop shaping controller is designed for stabilization, speed, throttle and yaw control. A constraint model based predictive control (MBPC) controller is implemented for longitudinal and lateral trajectory control. The results recorded in typical manoeuvres respect the performance criteria imposed.

1. Nomenclature

$u(1)$	$u(1) = F_1 + F_2 + F_3 + F_4$, N
$u(2)$	$u(2) = F_4 - F_2$, N
$u(3)$	$u(3) = F_3 - F_1$, N
$u(4)$	$u(4) = F_1 - F_2 + F_3 - F_4$, N
F_{xB}, F_{yB}, F_{zB}	Force in body-axis x,y,z direction, N
F_x, F_y, F_z	Force in earth-axis x,y,z direction, N
I_x, I_y, I_z	Moment of inertia in x,y,z direction
p, q, r	Roll rate,pitch rate,yaw rate, rad/s
ϕ, θ, ψ	Roll angle,pitch angle,yaw angle, rad
u_B, v_B, w_B	Velocity in body-axis x,y,z direction, m/s
u, v, w	Velocity in earth-axis x,y,z direction, m/s
x,y,z	COG in earth-axis x,y,z direction, m

2. Introduction

UAVs, or 'Unmanned Aerial Vehicles,' are defined as aircrafts without the onboard presence of pilots [11]. UAVs have been used to perform intelligence, surveillance, and reconnaissance missions. The technological promise of UAVs is to serve across the full range of missions. UAVs have several basic advantages over manned systems including increased maneuverability, reduced cost, reduced radar signatures, longer endurance, and less risk to crews. Vertical take-off and landing type UAVs exhibit even further maneuverability features. Such vehicles are to require little human intervention from take-off to landing.

Affordability is the key word when building and controlling a UAV. A commercial quad rotor helicopter, Draganflyer

[*]e-mail: mingc@ece.ubc.ca
[†]e-mail: huzmezan@ece.ubc.ca

III, was considered by our team as a starting point for more complex missions involving cooperative control and formation flying. This instrumented vehicle has significant autonomy required for prototype missions.

As regulatory design control method, H_∞ loop shaping has been picked since it combines classic loop shaping and the notion of bandwidth with model H_∞ robust stabilization. This technique extends the traditional parameter-space methods to enable the mapping of frequency response specifications into the parameter-space providing a straightforward way of selecting the gains in a fixed control structure to satisfy H_∞ robustness and performance specifications. This method, first proposed by McFarlane and Glover [7], has now been widely used in prototype aerospace projects. In 1994 [13], H_∞ loop shaping controller was used for position control of a radio controlled helicopter at hover. In 1996 [12], a fixed gain 2 degree of freedom H_∞ loop shaping controller was designed for the Westland Lynx multirole combat helicopter. In 1999 [8], a new linear parameter-varying (LPV) using also the 2 DOF H_∞ loop shaping design procedure was proposed to design a flight controller for the pitch dynamics of the VAAC Harrier. In 2001 [2], the 2 DOF control architecture and recent advances in parameter-space control design techniques were combined to form a new approach for designing flight controllers for high performance aircraft throughout a large design envelope.

After introduced in the late 1960's, Model Based Predictive Control (MBPC) has received much interest and been proven to be very successful in industrial applications. In [5], the MBPC scheme was applied to a linearized model of a high performance and high bandwidth aerospace process, and therefore can only be used around an operating point of the nonlinear process. Recent work has focused on extending MBPC strategy to a nonlinear high performance aerospace system [10][6]. The main advantage of MBPC is that the constraints can be easily handled, and therefore complex processes can be controlled without special precautions. In [9], the combined use of H_∞ loop shaping and MBPC architecture was motivated for designing automatic polits for civil aircraft.

The main reasons for introducing this scheme were:

- Same as the H_∞ flight controller, the MBPC controller can handle multivariable control problems naturally.

- The MBPC controller can take account of the actuator constraints and ensure the stability even if the constraints are exceed.

- It allows flight operation closer to the constraints compared with the H_∞ flight controller which can maximize

the tracking performance of UAVs.

- This combined architecture can perfectly integrate the robustness of the H_∞ controller for stability control and the constraint handling with the MBPC constrained trajectory control.

In this paper, we present in Section 3 the nonlinear quadrotor helicopter model. Next, in Section 4 the experimental flying mill is addressed. A briefing on the control methods is given in Section 5. A combined MBPC controller is designed in Section 6. The nonlinear simulation results proving the robustness and the satisfactory of the combined MBPC/H_∞ controller architecture are presented in Section 7 followed by conclusions in Section 8.

## 3. Nonlinear Quad-Rotor UAV Model
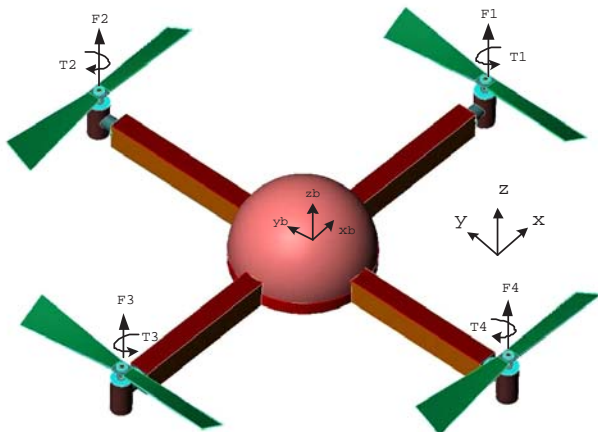
Figure 1: The Quad-Rotor UAV

The UAV used in the project is a commercial four-rotor helicopter, Draganflyer III, currently with a 3 min flying time but extensible to 1 hour by adequate sizing of the power source and actuators. Quad-rotor helicopters using the variant rotor speeds to change the lift forces are dynamically unstable and therefore a control law is permanently required to ensure their stability. Motions of the quad-rotor helicopter can be briefly described in Figure 1. The vertical motions along z-axis in the body-fixed frame can be obtained by changing the speeds of all the four rotors simultaneously. The forward motions along x-axis in the body-fixed frame can be achieved by changing the speeds of rotor 1 and 3 reversely and retaining the speeds of rotor 2 and 4. The lateral motions along y-axis in the body-fixed frame can be reached by changing the speeds of rotor 2 and 4 reversely and retaining the speeds of rotor 1 and 3. The yaw motions are related to the difference between the moments created by the rotors. To turn in a clock-wise direction, rotor 2 and 4 should increase speeds to overcome the speeds of rotor 1 and 3. The x,y axis definition becomes arbitrary since the structure presents x,y symmetry.

Section 1 summarizes the nomenclature used in the theoretical formulation and further in the SIMULINK model of the quad-rotor helicopter, Draganflyer III. This nomenclature is based on GARTEUR notations [1].

For convenience and compatibility with the control panel of the Futaba radio transmitter used with Draganflyer III, we define the inputs to be:

$$u(1) = F_1 + F_2 + F_3 + F_4$$
$$u(2) = F_4 - F_2$$
$$u(3) = F_3 - F_1$$
$$u(4) = F_1 - F_2 + F_3 - F_4$$

Thus, the motion equations of the quad-rotor UAV is:

$$\ddot{x} = \frac{u(1)(\sin\psi\sin\phi + \cos\psi\sin\theta\cos\phi)}{m} \quad (1)$$

$$\ddot{y} = \frac{u(1)(\sin\psi\sin\theta\cos\phi - \cos\psi\sin\phi)}{m}$$

$$\ddot{z} = \frac{u(1)\cos\phi\cos\theta}{m} - g$$

$$\ddot{\theta} = u(2)l/I_y$$

$$\ddot{\phi} = u(3)l/I_x$$

$$\ddot{\psi} = u(4)/I_z^{'}$$

where l is the length from the center of gravity of the helicopter to each rotor and m is the mass of the UAV. I represents the moment of inertia with respect to the axes and $I_z^{'}$ includes the moment of inertia of z axis and the force to moment scaling factor. The length l and mass m can be obtained by rule and balance. The moment of inertia in the x,y,z axes can be measured and identified using grey box identification. The drag coefficients were set to 0 in Equation 1 due to the relatively slow speeds at which this UAV operates.

The calculations of the above motion equations and the corresponding SIMULINK diagram are presented in [3].

4. The Experimental Setup
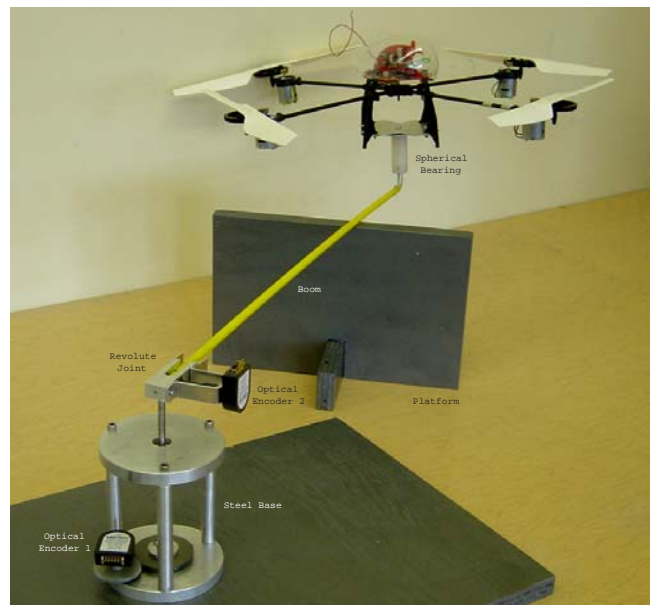
Figure 2: Photo of the flying mill with Draganflyer III

In order to carry out flight control experiments, an experimental rig including a custom designed flying mill, a personal computer, dSPACE DSP board, a microprocessor pulse modulator, a radio transmitter and the Draganflyer III was built.

A picture of the flying mill is shown in Figure 2. The steel base and carbon fiber boom limit the flight route of the UAV Draganflyer III to a half sphericity of 1 meter radius.

Two revolute joints at the base and near end of boom provide two degrees of freedom required for flight testing and system identification. In order to mitigate friction in the joints, the revolute joint at the near end of boom uses two low-friction radial ball bearings. The bearings are mounted in-line at an appropriate distance apart, parallel to their respective rotational axis, to minimize the moment loads. The far end of the boom is connected to a custom designed spherical bearing which provides the tested UAV enough tilted degrees of freedom and also prevents its four propellers from touching the ground or the boom. Due to the above features of this rig, the modelling and identification performed for the UAV did not justify the modelling of the flying mill. This spherical bearing is made of aluminum to reduce the payload of the tested UAV. The additional payload due to the weight of boom and the spherical bearing is approximately 60 g. The flying mill is mounted on a solid board to prevent overturning during the experiment or a catastrophic failure. Another platform is built to support the UAV during take off and landing. This platform can be replaced by limiting the UAV elevation.

Two optical encoders with resolution of 0.2 degree were used to sense the elevation and angles radial defining the UAV position. One optical encoder is fixed at the bottom of the steel base to record the rotational angle of the vertical shaft. Another optical encoder is mounted at the revolute joint at the near end of the boom to record the vertical position of the tested UAV. The two optical encoders are connected to the D/A dSPACE interface board, DS1102. During the experiment, the position of the UAV is provided by the data from the two optical encoders. The attitude data is updated by three gyroscopes on the UAV. The accelerations along three axes are given by the triaxial accelerometer also placed on the UAV. The encoders were used during the identification and validation of the UAV parameters.
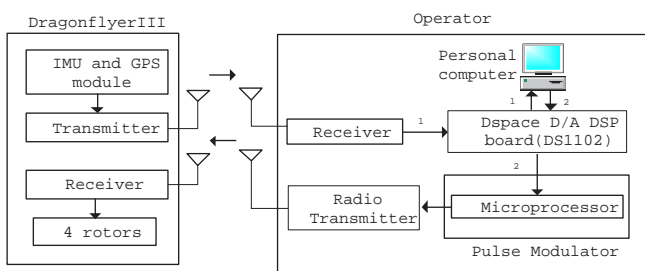

Figure 3: The Data Flow in Experimental System

Figure 3 shows the data flow in the experimental system. The attitude data and position data taken from IMU and GPS receiver module and the two encoders located on the flying mill, respectively, is transferred to dSPACE D/A interface board DS1102. Then, the data is analyzed by controller downloaded onto the dSPACE DS1102 processor. Control data can be generated either automatically, by the designed auto flight control laws, or manually, by the slider bars of the cockpit designed in the Control Desk of the dSPACE system. A microprocessor, PIC16F877, is programmed to transfer the control data to a pulse width modulated signal in order to reduce significant CPU load which otherwise would have been associated with the DS1102. This signal is further used to control the four rotors of the Draganflyer III via a 4 channel Futaba radio transmitter working in training mode. Currently no wireless connection between the flight control stationary computer an these sensors is used. This represents the subject of current work.

5. Briefing On The Flight Controller Design Method

5.1. MBPC

The basic strategy of MBPC is the repeated optimization of a performance objective over a finite horizon. It consists of the following three steps.

1. Given a reference trajectory $r(k + l)$ based on up to date time k, we assume $\widetilde{y}(k + l)$ as the l-step ahead predicted output over prediction horizon (N_y). This predicted output will be a function of future control increments $\Delta u(k + l)$ over control horizon (N_u), where $\Delta u(k + l) = u(k + l) - u(k + l - 1)$. For prediction, it is also assumed that $\Delta u(k + l) = 0$ for $l > N_u$.

2. Obtain the optimization of the cost function shown below.

$$J(k) = \sum_{l=1}^{N_y} \|\widetilde{y}(k+l) - r(k+l)\|_{Q(l)}^2 + \sum_{l=0}^{N_u} \|\Delta u(k+l)\|_{R(l)}^2$$

The weights $Q(l)$ and $R(l)$ are independent of k, but if a failure occurs they may need to vary with k. The norm $\|.\|_Q^2$ is defined as $\|.\|_Q^2 = x^T Q x$.

3. Minimize the above optimization by solving some standard algorithms such as Quadratic Programming subject to constraints on:

   - Input Levels: $u_l(l) \leq u(l) \leq u_u(l)$, where $k \leq l \leq k + N_u - 1$

   - Input Change Rates: $\triangle u_l(l) \leq \triangle u(l) \leq \triangle u_u(l)$, where $k \leq l \leq k + N_u - 1$

   - Output Levels: $y_l(l) \leq \widetilde{y}(l) \leq y_u(l)$, where $k \leq l \leq k + N_y$

4. Apply the first control signal of the sequence to the system, displace the horizon one time-step towards the future and repeat the procedure.

In order to obtain the predictions of the process output, an internal model based on the current measurements is needed. By using a linear model, the resulting optimization problem of the MBPC will be a quadratic program. If necessary, the cost function above could involve adjustable weights to compute the present control move such that the predicted output follows the reference in the desired manner.

5.2.   The 2 DOF H_∞ Loop Shaping

The internal model used in the MBPC design includes the stable model obtained through an H_∞ controller. This internal model takes advantage of the robustness and stability of the H_∞ flight controller to ensure better performance.

The general 2 DOF H_∞ controller scheme is shown in Figure 4. K_1 is the H_∞ controller for commands and tracking, and K_2 is the H_∞ controller for measurement or feedback signals. The shaped plant $G_s = W_2 G W_1$, with a normalized coprime factorization $G_s = M_s^{-1} N_s$. W_i gives exact model-matching at steady state. The design procedure of 2 DOF H_∞ loop shaping controller can be described as follows:
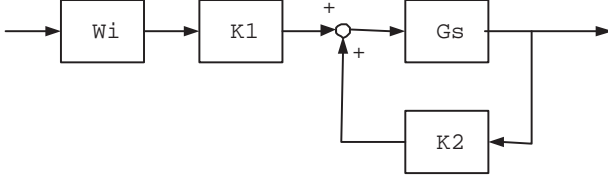
Figure 4: 2 DOF H_∞ Loop Shaping Controller

1. Loop Shaping: Assume G denotes the linear time-invariant model of the plant for design. Using frequency-dependent precompensator W_1 and/or a postcompensator W_2, the singular values of nominal plant G can be shaped to a designed open-loop shape and a specific loop bandwidth. The shaped plant G_s is defined as $G_s = W_2 G W_1$. The postcompensator W_2 contains low–pass and lead-lag filters for noise rejection and robustness augmentation. The precompensator W_1 contains proportional and integral (PI) filters. The proportional parts can reduce the phase lag around crossover and set the actuator range. The integral parts can improve the disturbance rejection ability.

2. A desired closed-loop transfer function T_{ref} between the commands and controlled outputs is selected.

3. Robust Stabilization: The stability margin ε :

$$\varepsilon^{-1}\rho^{-2} = \|(I - G_s K_2^{-1} G_s K_1 - T_{ref}\|_\infty$$

is calculated.

If the stability margin is in the interval [0.3, 1], the H_∞ controller K_∞ would guarantee robustness based on theoretical [7] and practical experience [8]. If the stability margin is not stratified, a return to (1) and an adjustment of W_1 and W_2 or T_{ref} is required.

4. Implementation: The 2 DOF controller K_1 and K_2 are then constructed by splitting the $K_\infty = \begin{bmatrix} K_1 W_i & K_2 \end{bmatrix}$ The resulting closed-loop system is simulated to verify the system stability and robustness. Iterations may be required.

6.   The Combined MBPC/H_∞ Controller Design

In the combined MBPC/H_∞ scheme, the stability augmentation system, which provides robust stabilization, disturbance rejection, noise rejection and the system decoupling, includes the inner loop and the speed, throttle and yaw outer loop. This fast dynamic system can be perfectly controlled by the H_∞ flight controllers. To ensure the good performance of the longitudinal and lateral channel even in the large manoeuvres, which exceeds the constraints of the actuators, the model based predictive control (MBPC) is implemented in the second outer loop. Note that since the throttle range of our UAV is very limited that normally does not cause the saturation of the actuators, only longitudinal channel and lateral channel are considered by the MBPC flight controller combined with the H_∞ flight controller.

6.1.   The Roll and Pitch Angles, Yaw Rate and Vertical Speed Stabilization Inner Loop 2 DOF H_∞ Controller
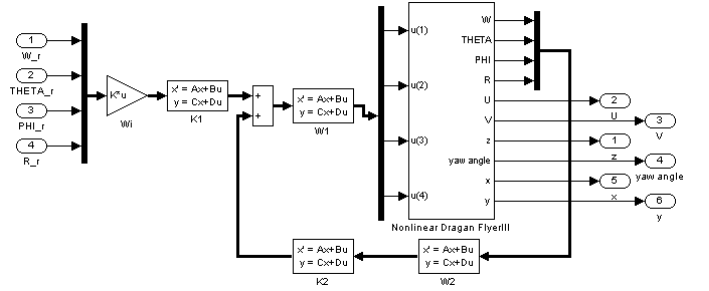

Figure 5: 2 DOF H_∞ Controller Inner Loop

The objective of the inner loop controller is to achieve decoupled robust stability control of the quad-rotor helicopter, Draganflyer III, at hover in disturbed air. The decoupling can further guarantee the use of diagonal H_∞ controllers for flying a specified trajectory. The 2 DOF H_∞ controller inner loop shown in Figure 5, used to control the attitude angles and vertical velocity, provides stabilization and decoupling as implemented in [4]. The reference values are the vertical velocity (W_r), the pitch angle (THETA_r), the roll angle (PHI_r), the yaw rate (R_r). Its control inputs are the pedal, the longitude, the latitude and the yaw controls. This controller should fulfil the following requirements:

- All the closed loop poles must lie in the left half of the s plane to ensure the stability and robustness.

- The closed-loop bandwidth should be set so that the rising time in each loop is around 2 seconds.

- The stability margin ε is to be in the interval [0.3, 0.4] allowing for 30-40 % coprime factor uncertainty.

- Quick pulse and step disturbance rejection.

The design procedure can be described as follows:

1. Linearize Model:
The nonlinear Draganflyer III model in [3] has to be reduced to the four loops required in this design to eliminate all redundant eigenvalues which make the Riccati equation unsolvable. The linear model is obtained by linearizing the nonlinear model around $u = \begin{bmatrix} 4.9 & 0 & 0 & 0 \end{bmatrix}^T$ equilibrium point. This is equivalent to freezing the scheduling states of the nonlinear controller around these control values.
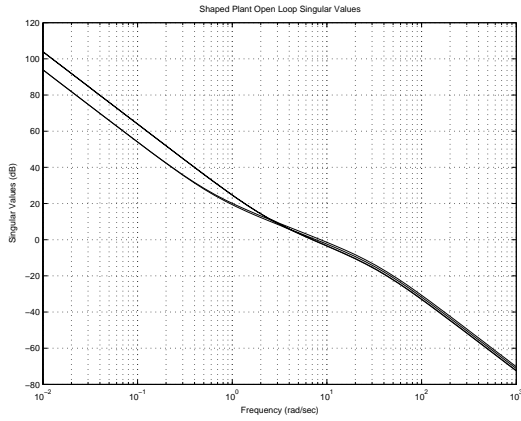
Figure 6: Inner Loop Singular Values of Shaped Plant

2. Loop Shaping:
Using frequency-dependent precompensator W_1 and a postcompensator W_2, the singular values of the shaped plant G_s, which is defined as $G_s = W_2 G W_1$, can be shaped to the designed open-loop shape and crossover frequencies at around 7 rad/s in Figure 6. The diagonal precompensator W_1 contains proportional and integral (PI) filters. The proportional parts can reduce the phase lag around crossover and set the actuator range. The integral parts can improve the disturbance rejection ability. The postcompensator W_2 contains first-order low-pass filters for noise rejection and robustness augmentation and the LHP zeros in pitch angle and roll angle loops to guarantee the slope of -1 in crossover region. The expressions for W_1 and W_2 are as follows:

$$W_1 = diag \left[\frac{1.52s+0.965}{s} \quad 13 \quad 13 \quad \frac{1.5(17.2s+9.7)}{s} \right]$$

$$W_2 = diag \left[\frac{90}{s+35} \quad \frac{73(s+2.31)}{s+35} \quad \frac{73(s+2.31)}{s+35} \quad \frac{90}{s+35} \right]$$

Since the architecture of pitch angle and roll angle loops are identical, the singular values of these two loops overlap. Therefore during controller tuning, the parameters of these two loops should keep the same, otherwise $u(2)$ and $u(3)$ would oscillate heavily around the equilibrium point.

3. Robust Stabilization:
To reach the objective rising time, the reference closed-loop transfer function T_{ref} was chosen to be:

$$T_{ref} = diag \left[\frac{1}{s^2+2s+1} \quad \frac{9}{s^2+5.7s+9} \quad \frac{9}{s^2+5.7s+9} \quad \frac{9}{s^2+5.7s+9} \right]$$

The H_∞ synthesis gave $\varepsilon = 0.3532$ which guarantees the robustness and stability of the inner loop controller.

4. Implementation:
The controller architecture is presented in Figure 5. The final H_∞ controller, K_∞ was split to $\begin{bmatrix} K_1 W_i & K_2 \end{bmatrix}$ which each has 4 inputs and 4 outputs. The W_i equals to $diag \begin{bmatrix} 1.2863 & 10.132 & 10.145 & 1.2885 \end{bmatrix}$

Figure 7 shows the closed-loop sensitivity function S for the inner loop H_∞ designed controller. The peak gain, which

is 2.29 dB at 14.6 rad/sec, allows for good disturbance rejection and reference tracking. The closed-loop complementary sensitivity function T is plotted in Figure 8. Its peak gain, 1.64 dB at 2.73 rad/sec, guarantees good noise rejection.
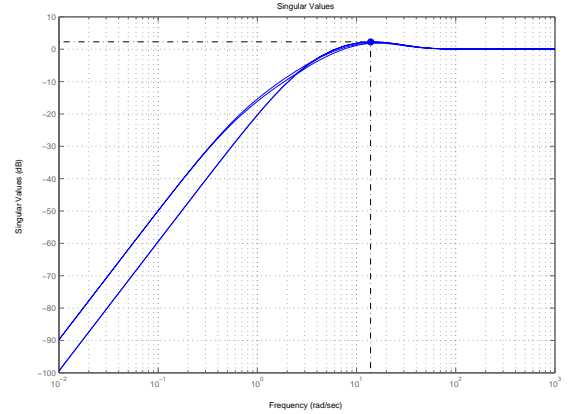

Figure 7: Inner Loop Closed-loop Sensitivity
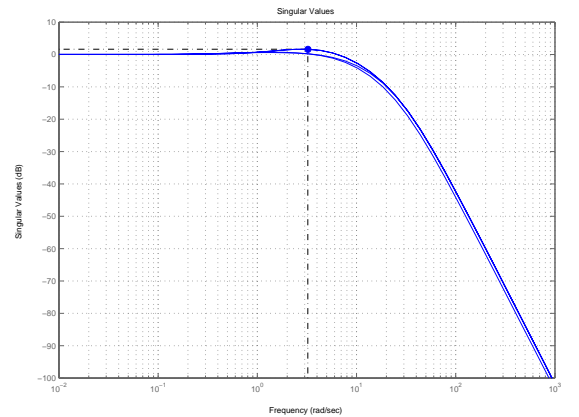
Figure 8: Inner Loop Complementary Sensitivity

6.2. Longitudinal and Lateral Speed, Throttle and Yaw Angle Outer Loop 2 DOF H_∞ Controller

The speed, throttle and yaw control outer loop, also called the first outer loop, was designed as in Figure 9. The reference values are the vertical position (Z_r), the x direction velocity in earth-fixed frame (U_r), the y direction velocity in earth-fixed frame (V_r), the yaw angle (PSI_r) and its control inputs are the vertical velocity (W_r), the pitch angle (THETA_r), the roll angle (PHI_r), the yaw rate (R_r), which are the reference values of the inner loop design. The required rising time in each loop should be around 4 seconds.

The design procedure can be presented as follows:

1. Linearize Model:
The nonlinear model of the inner loop and the Dragan-flyer III, see in Figure 10, was linearized around $u = \begin{bmatrix} 0 & 0 & 0 & 0 \end{bmatrix}^T$ equilibrium point.
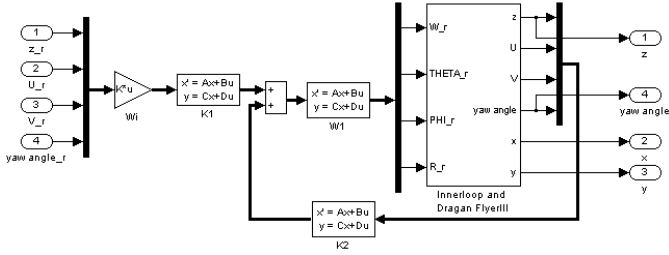
Figure 9: The First Outer Loop With H_∞ controller
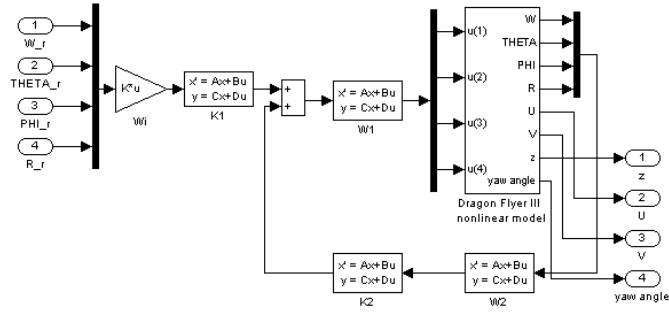
Figure 10: Nonlinear Inner Loop & Draganflyer III Model

2. Loop Shaping:

Since the Draganflyer III model has already been shaped desiredly in the inner loop design, only the diagonal pre-compensator W_1 with proportional gains is used to shape the singular values. The singular values of the shaped linear model are drawn in Figure 11. The crossover frequency is set to around 0.47 rad/s. The expression for W_1 is $W_1 = diag \begin{bmatrix} 0.5 & 0.05 & 0.05 & 0.5 \end{bmatrix}$.
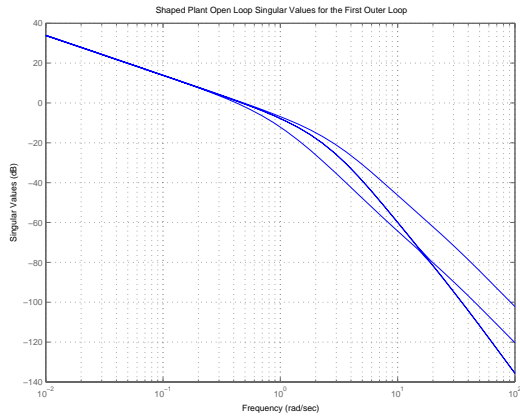
Figure 11: First Outer Loop Shaped Singular Values

3. Robust Stabilization:

The reference closed-loop transfer function T_{ref} was chosen as T_{ref} with the following diagonal entries:

$$\begin{bmatrix} \frac{1.69}{s^2+2.6s+1.69} & \frac{1.69}{s^2+2.6s+1.69} & \frac{1.69}{s^2+2.6s+1.69} & \frac{4}{s^2+4.2s+4} \end{bmatrix}$$

. The H_∞ optimization gave $\varepsilon = 0.3852$ which guaran-

tees the robustness and stability of the first outer loop controller.

4. Implementation:

The Simulink Diagram in Figure 9 was implemented to check the performance of the achieved controller. The final H_∞ controller, K_∞, which has 64 states, 8 inputs and 4 outputs was first reduced to 20 states, 8 inputs and 4 outputs. Then the reduced H_∞ controller was split to K_1 and K_2 which each has 4 inputs and 4 outputs. $Wi = diag \begin{bmatrix} 1.825 & 1.656 & 1.656 & 2.1116 \end{bmatrix}$ contains the static steady gain for each loop.
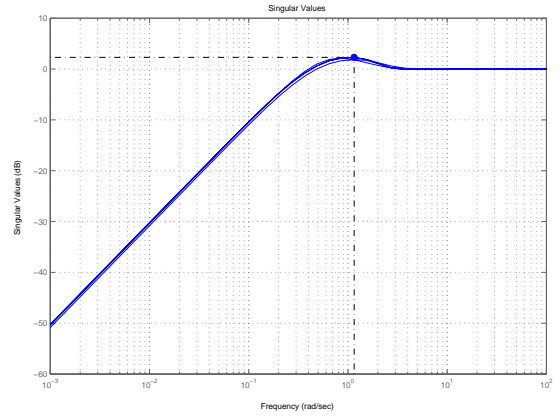
Figure 12: First Outer Loop Sensitivity
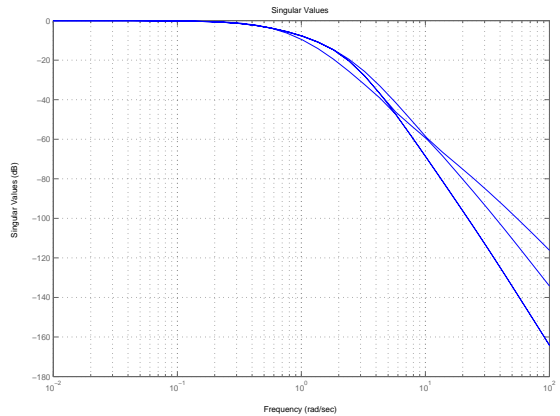
Figure 13: First Outer Loop Complementary Sensitivity

The closed-loop sensitivity function S in Figure 12 indicates good disturbance rejection achieved by the H_∞ controller. The peak value is 2.31 dB at the frequency of 1.06 rad/s. Figure 13 shows the closed-loop sensitivity function proving the good noise rejection exhibited by the H_∞ controller.

6.3. Constraint MBPC Trajectory Controller

The trajectory longitudinal and lateral outer loop are closed with the MBPC controller is shown in Figure 14. The internal model was linearized from the nonlinear model that includes the Draganflyer III, the inner loop and first outer loop
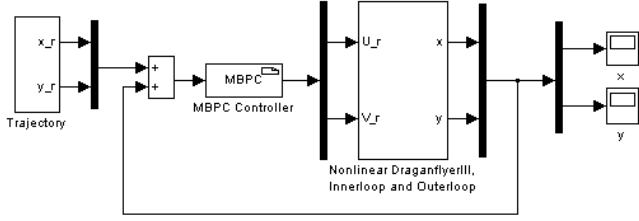
Figure 14: MBPC In Longitudinal And Lateral Channel

both achieved with the 2 DOF H_∞ controller, see in Figure 15. After linearization, the longitudinal and lateral speed channels were selected for the MBPC design. The prediction horizon was set to 10 and the control horizon was 1 to ensure a fast response. The output weight was $Q = diag \begin{bmatrix} 5 & 5 \end{bmatrix}$ and the input weight was $R = diag \begin{bmatrix} 1 & 1 \end{bmatrix}$. Constraints on the longitudinal and lateral speeds and the rate change of the two speeds have been implemented.
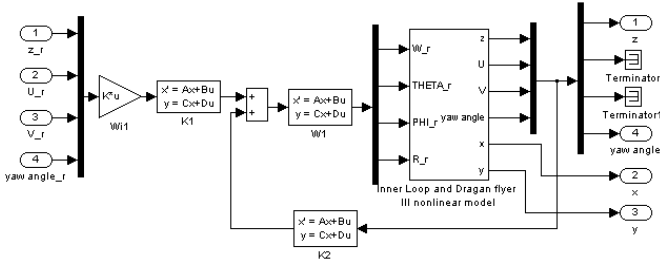
Figure 15: Nonlinear Model of The Second Outer Loop

7. Results

The achieved controller in each loop was simulated to check its robustness and stability.

The performance of the stabilization inner loop with the 2 DOF H_∞ controller is checked in Figure 16 and Figure 17. Figure 16 compares the nonlinear step responses of each loop separately with the H_∞ controller in place. The rising time of each step response is around 2 seconds, satisfying the specification. Figure 17 shows the output step disturbance to each loop. The outputs return to zero after 2-3 seconds indicating very good step disturbance rejection of the controller. Such fast responses are prone to actuator saturation.

The performance of the speed, throttle and yaw control outer loop with H_∞ controller is checked in Figure 18 and Figure 19. Figure 18 compares the step response to each loop with the H_∞ controller in place. For the vertical position (z) loop, the rising time is about 5 seconds. For the x and y direction velocity loops (U and V) loops, the rising time are all around 4.5 seconds. The rising time of the yaw angle loop is around 3.5 seconds. The controller designed specifications of the Draganflyer III are met. Figure 19 shows that the output step disturbance to each loop was also rejected quickly by the H_∞ controller.

Figure 20 shows the nonlinear simulation of large manoeuvres in the longitudinal and lateral channel. The constraints
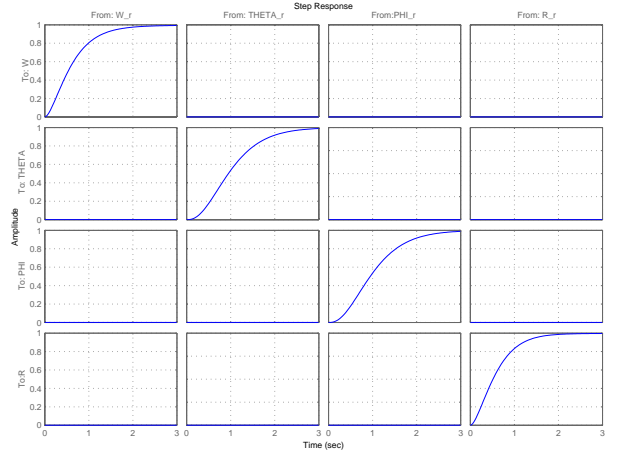

Figure 16: Inner Loop Step Responses
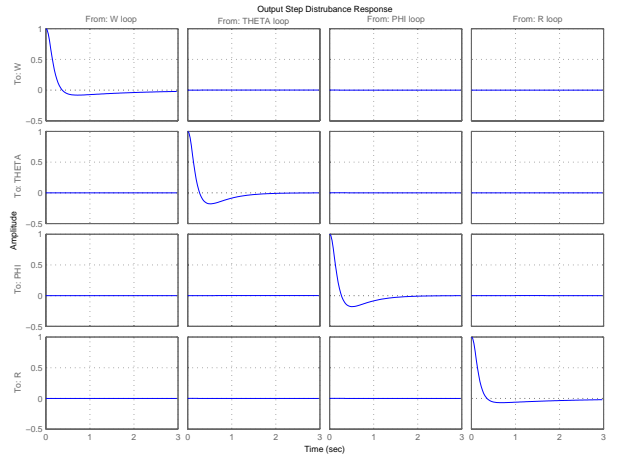


Figure 17: Inner Loop Output Step Disturbance Responses
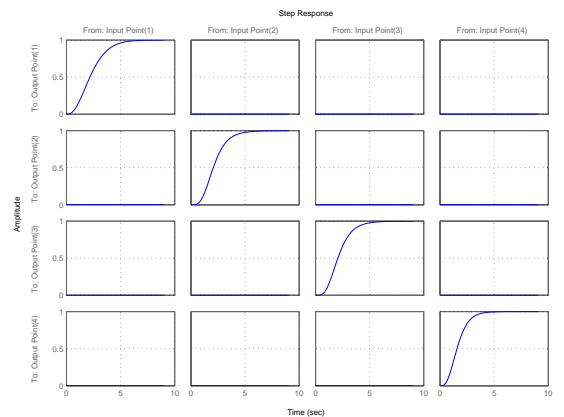

Figure 18: First Outer Loop Step Responses
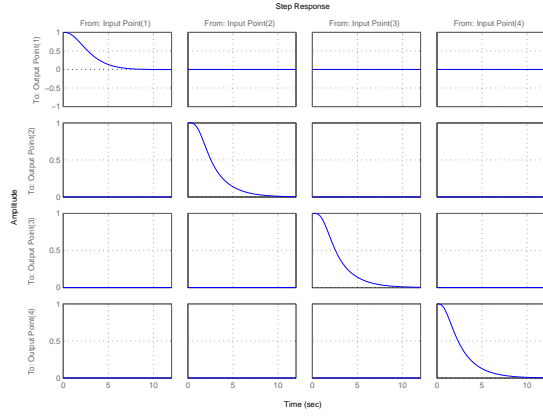
Figure 19: First Outer Loop Step Disturbance Responses

of control inputs are $-2m/s \le U\_r \le 2m/s$, $-2m/s \le V\_r \le 2m/s$, $-1m/s \le \Delta U\_r \le 1m/s$ and $-1m/s \le \Delta V\_r \le 1m/s$. The reference value in the longitudinal channel is 60 meters and the reference value in the lateral channel is -40 meters. The inputs, U and V, saturates during the flight time. From this simulation, we conclude that the MBPC architecture improves the constraint handling ability of the autonomous UAV.
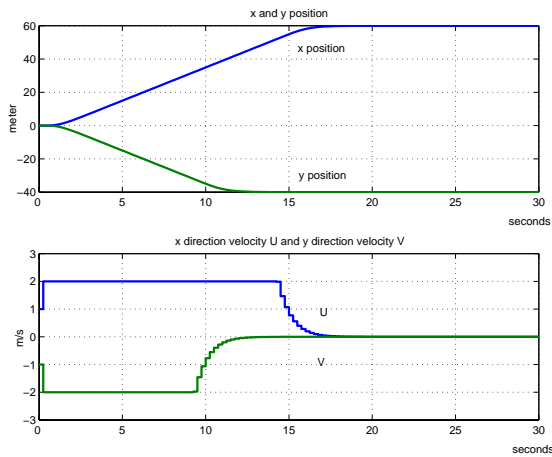
Figure 20: Large Step Responses In The Longitudinal And Lateral Channel With Constraint MBPC

To check the combined MBPC/2 DOF H_∞ controller, a nonlinear trajectory simulation was implemented as in Figure 21. The reference values are the x direction position, y direction position, z direction position in earth-fixed frame and yaw angle. The initial position of Draganflyer III was at (0,0,0) in the earth-fixed frame with 0 degree yaw angle. First, the Draganflyer III was asked to fly to (8,6,3) meters with 0 degree yaw angle. At 15 seconds, the UAV flew to the next destination at (11,12,11) meters. At 30 seconds, the UAV changed its yaw angle to 30 degree while keeping this hover position unchanged. Figure 24 shows the step responses of this trajectory simulation of each loop. All control values reached the reference values within 5 seconds.

Two trajectory scenarios were simulated with the com-
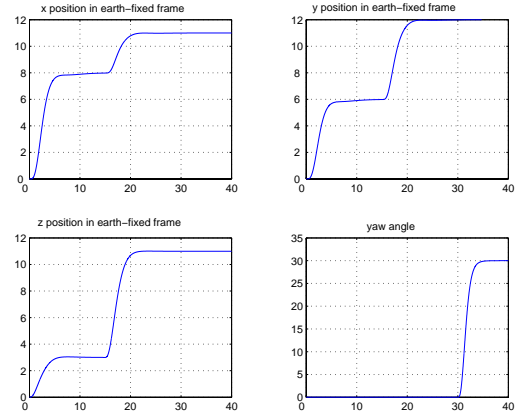
Figure 21: Trajectory Step Response With The Combined MBPC/2 DOF H_∞ Controller
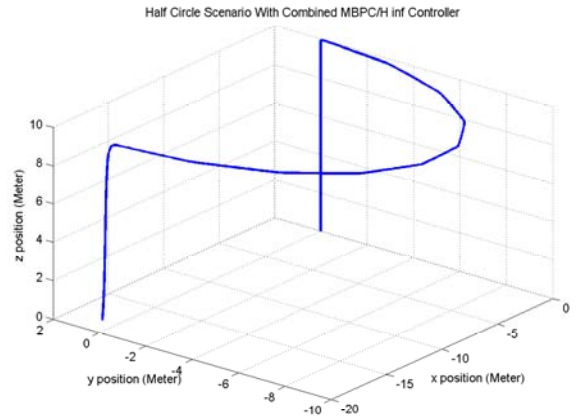
Figure 22: Half Circle Scenario With The Combined MBPC/2 DOF H_∞ Controller
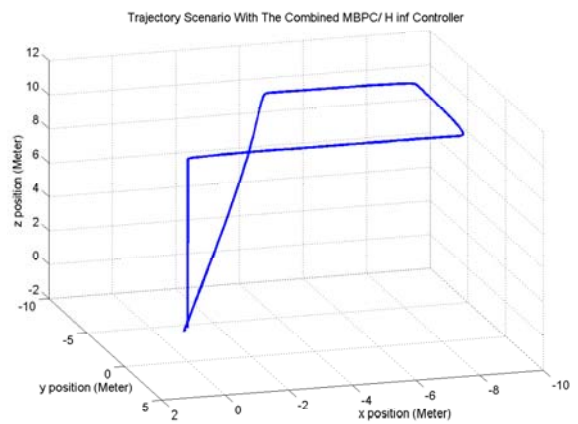
Figure 23: Trajectory Scenario With The Combined MBPC/2 DOF H_∞ Controller

bined MBPC/2 DOF H_∞ controller in Figure 22 and Figure 23. Figure 22 shows the half circle trajectory. After vertically taking off from (0,0,0) to (0,0,10) meters , the Draganflyer III flew to (-20,0,10) meters through a half circle trajectory. Then, the UAV vertically landed. Figure 23 animates the other trajectory scenario. After vertically taking off from (0,0,0) to (0,0,10) meters, the Draganflyer III flew to (-9,0,10) meters. Then, the UAV flew to the next two destinations at (-9,-8,10) and (-4, -8,10) meters continuously. Finally, the Draganflyer III flew back to the original point at (0,0,0).

8.   Conclusions

In this paper, we have presented an automatic quad-rotor UAV design. A high fidelity nonlinear model was obtained and represented in SIMULINK for design purpose. A testing flying mill was built for the flight testing and parameter identification. Based on the nonlinear model, an H_∞ loop shaping controller was designed for the robust stability and trajectory control. To improve the constraint handling ability for large manoeuvres , a combined MBPC/H_∞ controller was employed. Nonlinear simulations have shown this combined architecture yields satisfactory performance in the presence of disturbances and various input and /or output constraints. Flying mill simulations are currently on the way.

References

[1] *Robust Flight Control Design Challenge Problem Formulation and Manual.* Group For Aeronautical Research And Technology In Europe.

[2] Paul Blue, Levent Güvenc, and Dirk Odenthal. Large envelope flight control satisfying H_∞ robustness and performance specifications. *Proceedings of the American Control Conference, Arlington,VA*, June 25-27,2001.

[3] Ming Chen and Mihai Huzmezan. A simulation model and H_∞ loop shaping control of a quad rotor unmanned air vehicle. *Modelling and Simulation 2003,IASTED International Conference, Palm Springs, California,USA*, 380-203, February 2003.

[4] M. L. Civita, G. Papageorgiou, W. C. Messner, and T. Kanade. Design and flight testing of a gain-scheduled H_∞ loop shaping controller for a robotic helicopter. *Submitted to the 2003 American Control Conference.*

[5] S. A. Heise and J. M. Maciejowski. *Model Predictive Control of a Supermaneuverable Vehicle.* In Proceedings of the AIAA Guidance, Navigation and Control Conference, 1996.

[6] H. Jin Kim, David H. Shim, and Shankar Sastry. Nonlinear model predictive tracking control of rotorcraft-based unmanned aerial vechicles. *Proceedings of the American Control Conference, Anchorage, AK*, May 8-10,2002.

[7] D. McFarlane and K. Glover. A loop shaping design procedure using H_∞ synthesis. *IEEE Trans. on Automatic Control*, 37, June,1992.

[8] G. Papageorgiou and K. Glover. Taking robust LPV control into flight on the VACC Harrier. *Proceedings of the 39th IEEE conference on Decision and Control*, pages 4558–4564, 2000.

[9] G. Papageorgiou, M. Huzmezan, K. Glover, and J. Maciejowski. Combined MBPC/H-inf autopilot for a civil aircraft. *Proceedings of ACC'97, June 1997, Albuquerque, USA.*

[10] C. M. Shearer and S. A. Heise. Contrained model predictive control of a nonlinear aerospace system. *AIAA*, page 4235, 1998.

[11] UAVs. New world vistas: Air and space for the 21st centry. *Human systems and biotechnology systems*, 7.0:17–18, 1997.

[12] D. Walker and I. Postlethwaite. Advanced helicopter flight control using two-degree-of-freedom H_∞ optimization. *Journal of Guidance, Control and Dyanmics*, 19:461–468, 1996.

[13] Martin F. Weilenmann, Urs Christen, and Hans P. Geering. Robust helicopter postion control at hover. *Proceedings of the American Control Conference, Baltimore,Maryland*, June 1994.